Large Eddy Simulation in Three-dimensional Cavity Using Dynamic Modeling

A. F. A. PINHO[1], J. G. COELHO*[1] and A. S. NETO[2]
[1]University of Triangulo Mineiro
Department of Mechanical Engineering,Rua Randolfo Borges Junior, 1255, Uberaba, Brazil
[2]University of Uberlandia
Department of Mechanical Engineering, Av. Joao Naves de Avila, 2121, Uberlandia, Brazil
*Correspondence author: josegustavo@icte.uftm.edu.br

Abstract: Our study developed a fourth-order numerical code in space and a third-order in time with dynamical turbulence model. This code was applied to study turbulence transition in shear driven cavity flow in bi and three-dimensional configurations. The simulations had been carried out for bi and three-dimensional configurations. The two dimensional simulations were performed to be compared with results presented in the literature in order to validate the developed code, as well as to define the best parameters for the simulations in three-dimensional configuration. The Reynolds numbers were taken as 3200, 10000, 25000, 50000 and 100000. The simulations of cubic shear driven cavity flow with Reynolds numbers 3200 and 10000 were compared with results presented in the literature. Two-dimensional simulation was performed without turbulence model, and three-dimensional simulations were performed using the Smagorinsky and Germano models for sub-grid scale. The topological physical nature was analyzed and some important new physic characteristics were pointed out.

Key–Words: LES, Simulation, Cavity

1 Introduction

In the mid-twentieth century, researchers had great interest in flows in rectangular cavities with sliding lid. This is evidenced by [1], one of the pioneers at studying this problem numerically, and [2], who conducts numerical and experimental studies. Moreover, recent works such as [3] and [4] indicate that this geometric configuration continues to arouse interest. In the first study, the authors conducted a numerical study in a cubic cavity flow with a Reynolds number of 1000. The latter is a numerical study on the transition from laminar flow to chaotic in two-dimensional configuration.

Among the practical applications of the flow in shear driven cavity, we have liquid fllms deposition process on a surface [5]. Another application indicated by [6] is the smelting flow within the cavities used for the manufacture of microcrystalline materials. Regarding the flow of which the cavity is an idealization, we can mention the flow of notches and slots on repeated heat exchangers walls or surfaces of aircraft bodies [7].

A critical point for the development of modern engineering and for understanding the physics of turbulent flows is the analysis of the progress and topology of flows. In this context, numerical simulations are more accurate for detailed experimental measurements of the flow, such as confirmation of the lateral vortices obtained in the laboratory ([8]). As the Reynolds numbers is nearly 1300, it is considered that the flow in shear driven cavity enters transient, but still laminar ([5] and [8]). The transition to turbulence occurs at a Reynolds number between 6000 and 8000. The transition to turbulence occurs at a Reynolds number between 6000 and 8000, in different regions of space, starting in the region of the posterior secondary vortex ([9] and [6]). For Reynolds number above 10000, the flow is completely turbulent.

Among experimental works in cavities, it is worth mentioning the studies of [10]; the authors performed experiments using injection and particulate ink display to visualize and study the flow in wells with Reynolds number of 1000, and transverse aspect ratio of 2:1. The obtained results indicated that injection of ink at initial flow velocities in the cross direction of the side walls propagate to the plane of symmetry.

In terms of Large Eddy Simulation (LES), we have a work by [11]. This study compares results obtained with the Smagorinsky model using various wall models and the results obtained with the dynamic Germano model. The article [12] proposed the dynamic sub-grid model, and the authors state that the Smagorinsky model is the most commonly applied sub-grid model; still, they review the Smagorinsky

constant values previously employed, concluding that it is impossible to simulate the entire range of phenomena present in the fluid flows using only a universal constant.

The objective of this study is to analyze these transient structures in flows in shear driven cavity with Reynolds number of 10000, 25000, 50000 and 100000. For this study, we developed a computational code of finite differences to the solution of the Navier-Stokes equations for incompressible flow with constant properties. This code was implemented with different second- and fourth-order centered discretizations for the velocity and Smagorinsky and Germano sub-grid models. Initially, tests were performed in two-dimensional configuration with Reynolds numbers 1000, 3200, 5000 and 10000. These tests established the program parameters, mesh to be used, form of discretization, solver, etc. Subsequently, simulations were performed in three-dimensional configuration. We simulated a stationary case with Reynolds number of 1000; and if the Reynolds number is 3200, which is considered laminar. This case was designed to validate the code in three-dimensional configuration. The objective of the cases used in this study and the simulation of flow Reynolds number of 10000 was to verify the performance of sub-grid Smagorinsky model and dynamic sub-grid Germano model. As the latter presented the most satisfactory results. it was applied in the simulations of flow Reynolds number of 25000, 50000 and 100000.

2 Mathematical Formulation

The governing equations for the proposed problem is the continuity and momentum equations. By applying the filter, we obtain

$$\frac{\partial u_j}{\partial x_j} = 0 \tag{1}$$

$$\frac{\partial u_j}{\partial t} + \frac{\partial u_j u_i}{\partial x_j} = \frac{1}{\rho}\frac{\partial p}{\partial x_j} + \frac{\partial}{\partial x_j}(\upsilon\frac{\partial u_i}{\partial x_j} - \tau_{ij} + \alpha_{ij} + f_i). \tag{2}$$

where ∂ is the Partial differential operator, u the velocity component, t the time, ρ the density, υ the kinematic viscosity, τ_{ij} the sub-grid tensor and α_{ij} the Cross term of Navier Stokes equation.

For the turbulence, Boussinesq (1877) proposed a sub-grid tensor model similar to the model of viscous strains. For this purpose, the concept of eddy viscosity in the boundary layer on an infinite flat plate. Kolmogorov (1942) proposed a generalized form of the hypothesis Boussinesq, which became the method currently applied [13], submitted in Eq. 3

$$\tau_{ij} = -2\upsilon S_{ij} + \frac{2}{3}\delta_{ij}\tau_{ij}. \tag{3}$$

where S_{ij} is deformation tensor and δ_{ij} the Kronecker delta.

Smagorinsky, following the idea of mixing length model Prandtl [14] proposed a sub-grid model with eddy viscosity proportional to the characteristic length of mesh at a characteristic sub-grid speed . Length of the mesh is an obvious choice; speed should be related to the speed of small scales of the order of speed variation on a mesh element [13]. Therefore, eddy viscosity is

$$\upsilon_t = (C_S\Delta)^2\sqrt{2S_{ij}S_{ij}} \tag{4}$$

where υ_t is the eddy viscosity and C_s the Smagorinsky constant

For flows near the walls, this model fails since the deformation rates in this region are very high, generating elevated values to the eddy viscosity. However, these values should be low since turbulence decreases as it approaches the wall. The dynamic model proposed in [12] suggests an adjustment of the dynamic sub-grid model varying in space and time. Based on the Smagorinsky model, the Germano model adjusts an coefficient of proportionality between the eddy viscosity and the deformation tensor module. In this case, the coefficient is obtained by:

$$C = \frac{1}{2}\frac{L_{ij}M_{ij}}{M_{ij}M_{ij}} \tag{5}$$

where L_{ij} and M_{ij} are Germano tensors

2.1 Numerical Method

Our study used a fully explicit second-order method Adams-Bashforth for both advective and diffusion speed terms, and a fully explicit for pressure,

$$\frac{(\phi^{n+1} - \phi^n)}{\Delta t} = -G(p^{n+1}) + \frac{3}{2}[\phi^n)] - \frac{1}{2}[S(\phi^{n-1})] \tag{6}$$

where Φ is any of velocities, $G(p)$ the pressure gradient and $S(\Phi)$ the Advective terms.

Coupling pressure-velocity is carried out by using the method of pressure correction. A velocity field is estimated considering the pressure field in the previous time. The applied spatial discretization is centered differences for both advective and diffusive term. Differences used centered second- and fourth-order for

speed. The difference in the results obtained with the two discretizations are given in Results. For pressure, only second-order discretization was employed.

The cases studied in this work consist of cavities, therefore, we used exclusively the the wall with imposed speed condition. For the imposition of boundary conditions, we used the facilitation ofvirtual points consisting of points outside the domain [15].

In all of the studied cases, the solver used for the pressure equation was the modified strongly implicit procedure (MSIP), such as the formulation in [16].With this method, solving the linear system is a highly accurate, fast and robust procedure. The linear system is solved up to a pre-established minimum residue 10^{-6} for two-dimensional case, and 10^{-4} for three-dimensional cases.

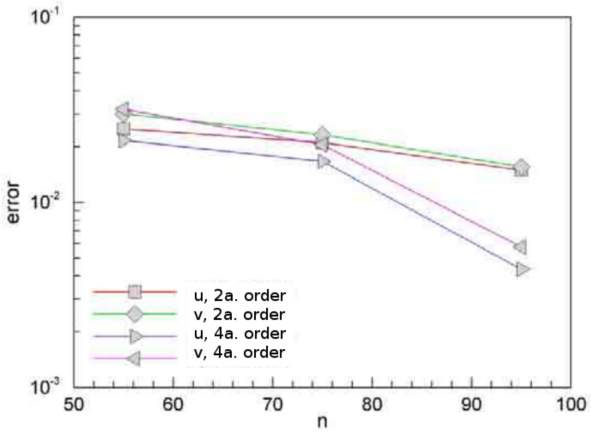

Figure 1: Mean error of velocity profiles for Reynolds number 10000 calculated in [17].

3 Results

3.1 Two-Dimensional Cavities

We simulated two-dimensional cases with Reynolds numbers of 1000, 3200, 5000 and 10000, obtained with second- and fourth-order discretizations and meshes with 55, 75 and 95 points in both directions. These comparisons were performed using the profile of the velocity component u in the cavity vertical center line (x = 0.5) and the profile of the velocity component v in a line horizontal to the cavity center (y = 0, 5).

For an analysis on the convergence order achieved with the discretization methods, we use the solutions obtained with Reynolds number of 10000. Since there is no steady state for this solution, the values indicate are averages of time; in all of the cases obtained between 1 and 3 seconds. Oscillations due to the initial transient were damped, with the flow statistically steady.

Figure 1 indicates the mean errors calculated through Eq. 7 with respect to the results of [17] for the solutions obtained for Reynolds number 10000. The solutions obtained with second-order discretization maintain this convergence throughout the range of the number of points shown for both the velocity component u as for component v. Regarding the solutions obtained with fourth-order discretization, we observed that the mesh solution obtained with 55 points in both directions for the obtained mesh with 75 points convergence is slightly larger than a second-order convergence. However, between the solution using 75-point mesh and 95-point mesh convergence reaches fourth order, which is probably due to the action of the boundary conditions of the second order, as explained in [18]

$$e = \frac{\sqrt{\sum (u_i - u)^2}}{n} \tag{7}$$

The results of this convergence can be observed by comparing the profiles of velocity components u (Fig. 2) obtained with 95-point mesh in both directions and with second- and fourth-order discretization. It appears that in the former, velocities do not reach maximum and minimum speeds, although capture the shape of the curve consistently; the latter approached the critical points established through reference results.

The mesh influence on the solution through fourth order discretization is illustrated in Fig. 3, with the profile of the velocity component of profile v. We can observe that only the solution through fourth-order discretization and 95x95 mesh reaches the critical points of the reference solutions; the remaining two solutions fail even to determine the positions of these points.

Since it was the only solution with results very close to the reference, it is preferable to use the 95x95mesh with fourth-order discretization is for simulations in three-dimensional cavities.

Figure 4 indicates the profiles of u velocity components for the solutions obtained with Reynolds number 1000, 3200 and 5000, obtained using fourth-order discretization and mesh with 95 points in both directions. The results are compared with [17]; the profiles proved to be in great accordance with each other. The average errors obtained were 10^{-5} for the solution of Reynolds number 5000.

Figure 5 illustrates the vorticity field superimposed by a set of flow lines indicating the center of

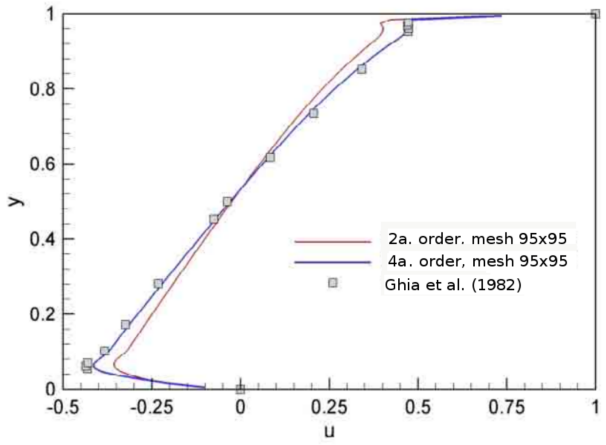

Figure 2: Comparison of velocity component profiles u at y = 0.5 Reynolds number 10000 obtained with 95 x 95 mesh.

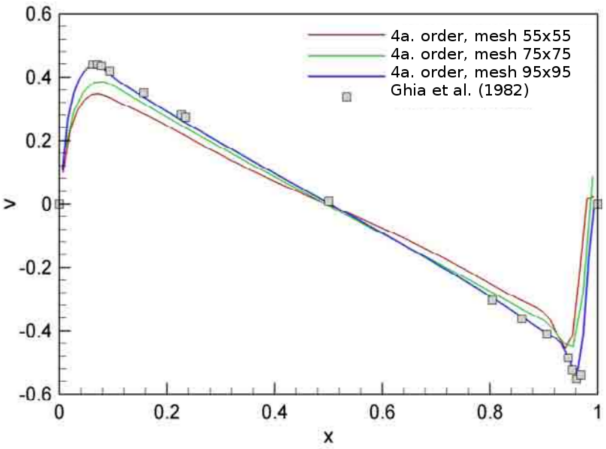

Figure 3: Comparison of velocity component profiles v at y = 0.5 for Reynolds number 10000 obtained with fourth-order discretization.

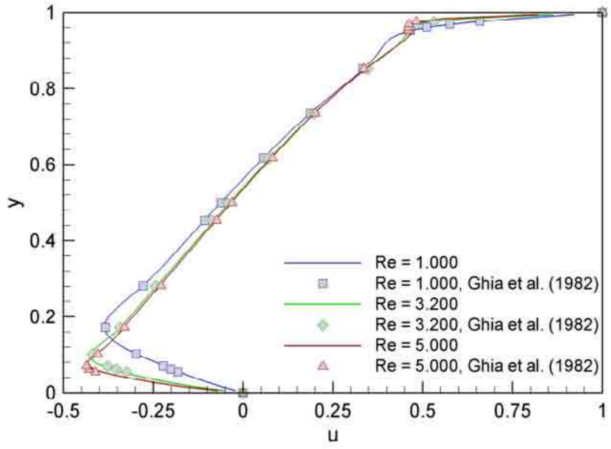

Figure 4: Comparison of the profiles of velocity component u x = 0.5 obtained with 95 x 95 mesh and fourth-order discretization.

structures formed for the case with Re = 5000. We clearly have central circulation secondary vortices on the lower corners, which becomes higher with increasing Reynolds number. Figures 6 and 7 indicate the average field obtained with discretization of second- and fourth-order, respectively,presenting little difference between them , except for the small vortex on the lower left corner, not presented in the solution of second- order discretization. This topology was predicted by [19].

3.2 Three-dimensional cavities

For tri-dimentional cavities, results were obtained regarding five cases - Reynolds of 3200, 10.000, 25.000, 50.000 and 100.000, with 95 x 95 x 65 mesh for all of the cases, time step of 0.005, and fourth-order discretization. Turbulent kinetic energy spectra were obtained using k signal by averaging temporal samples, numbering 8 per sample. The analysis of flow topology used current lines, isosurfaces of vorticity and criterion Q, which is is defined in [20].

The results obtained for flow Reynolds number 3200 are shown below. This simulation was performed with 0.001s time step. In Fig. 8, u profile is compared with both the experimental [7] results and the numerical [21] results, indicating good accordance, with a slight overestimate speed at minimum speed point of the u velocity component profile.

In Fig. 9, the root mean square of velocity (RMSv) profile is compared with the experimental results obtained by [7]. In Fig. 10, the experimental UV profile obtained is compared with the same authors re-

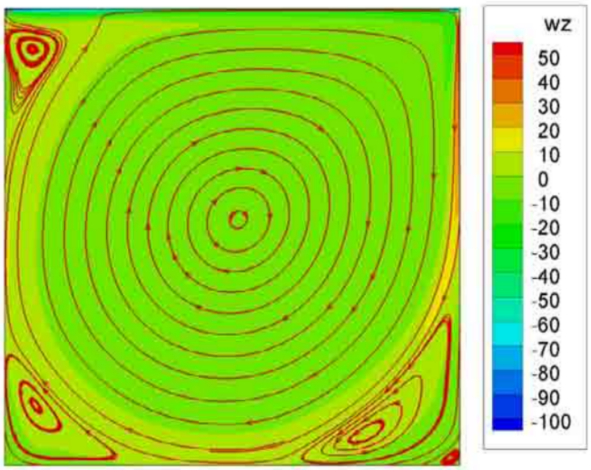

Figure 5: vorticity fields with superimposed streamlines in steady flow for Reynolds number 5000, obtained with discretization of fourth order, 95 x 95 mesh and time step 10^{-3}.

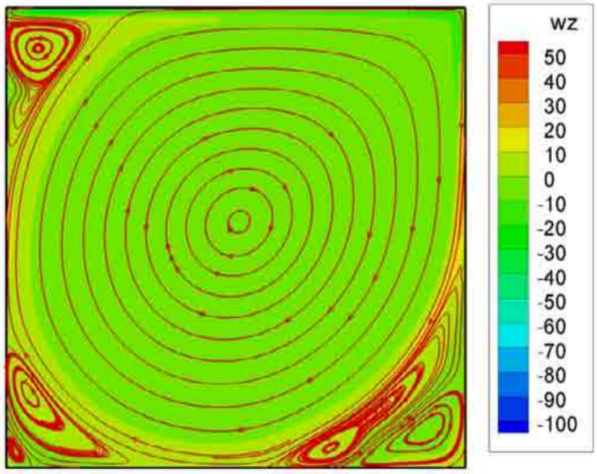

Figure 7: Average vorticity field with superimposed streamlines for Reynolds number 10.000, obtained with discretization of fourth-order and 95 x 95 mesh.

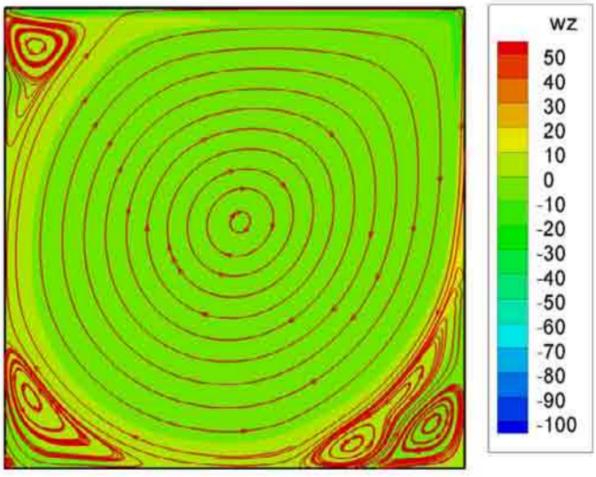

Figure 6: Average vorticity field with superimposed streamlines for Reynolds 10000, obtained with discretization of secound-order and 95 x 95 mesh

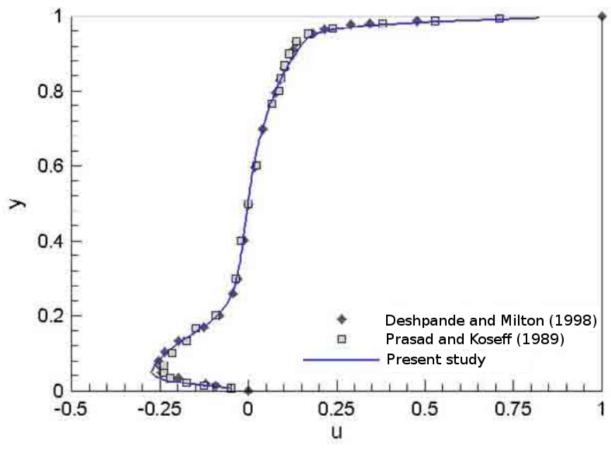

Figure 8: Comparison of component profiles of velocity u, z = 0.5 and x = 0.5 for Reynolds number 3200 with literature data.

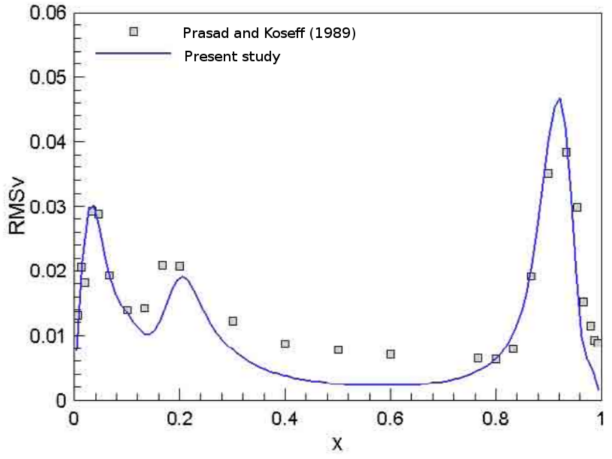

Figure 9: Comparison of RMSv profiles at z =0.5 and y = 0.5 for Reynolds number 3200 with literature data.

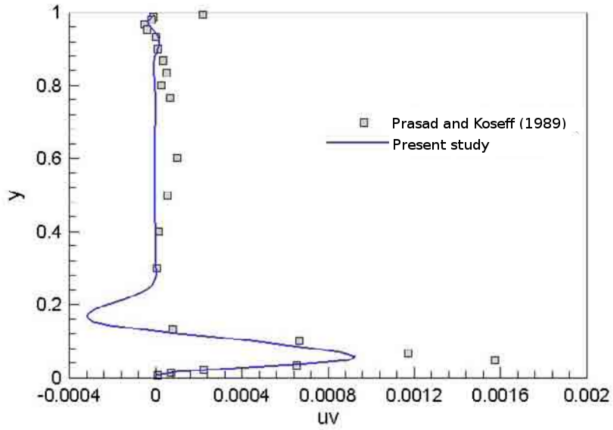

Figure 10: Comparison of UV profiles at z =0.5 and x = 0.5 for Reynolds number 3 20 0 with literature data.

sults, indicating a good accordance. We can observe that the shape of the profile is captured by the data; however, the fluctuation peaks are not achieved, especially in the turbulent region, as the top and bottom of the cavity.

The u profile obtained without sub-grid model, with Smagorinsky and the dynamic Germano model, is compared with the experimental results obtained by [7], illustrated in Fig. 11 indicating no significant differences in the obtained velocity profiles.

In Fig. 12, the RMSv profile obtained without sub-grid model, with Smagorinsky model and the dynamic Germano model are compared with the experimental results obtained in [7]. Figure 13, the UV profile obtained without sub-grid model with the Smagorinsky model and the dynamic Germano model are compared with experimental results obtained by the same authors. Observe a good agreement between the results shown.

The same observation is made for the profiles in the flow Reynolds number equal to 3200 can be performed in this case. However the dynamic Germano model best captures the curves format. The Samgorinsky model proves to be very diffusive, since this model redistributes the kinetic energy of the largest regions for smaller intensities. This can be seen, can be seen with greater intensity in Fig. 13.

Figure 14 illustrates the u profile obtained with the dynamic Germano model compared with the experimental results of the[7] and the numerical results of the [21]. It appears that the dynamic Germain model presents better correlation of the results for Reynolds numbers 10.000 than the absence of mod-

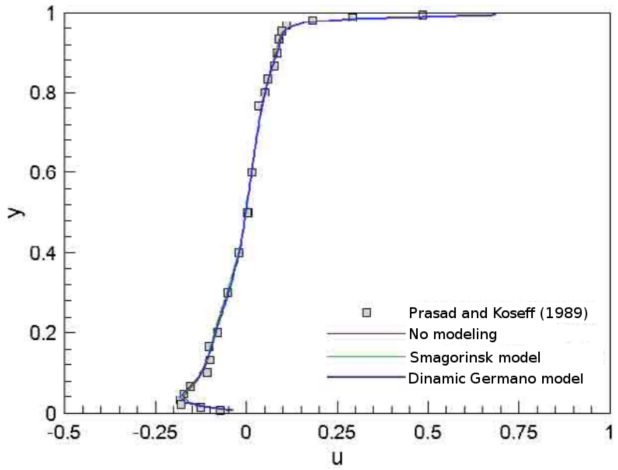

Figure 11: Comparison of profiles of velocity component u, z = 0.5 and x = 0.5 for Reynolds number 10000 with literature data.

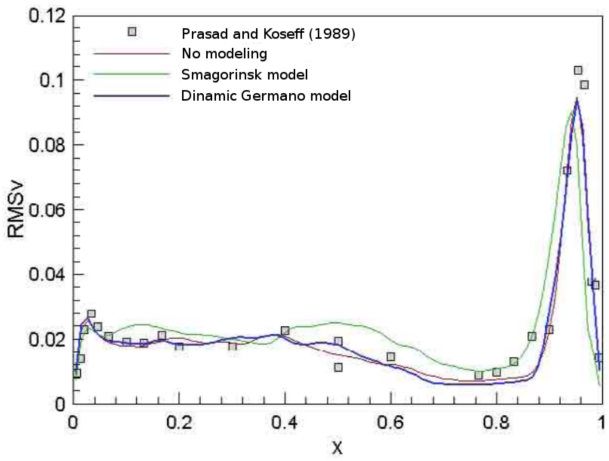

Figure 12: Comparison with literature data and between the profiles of RMSv z= 0.5 and y = 0.5 for the same Reynolds number 10,000.

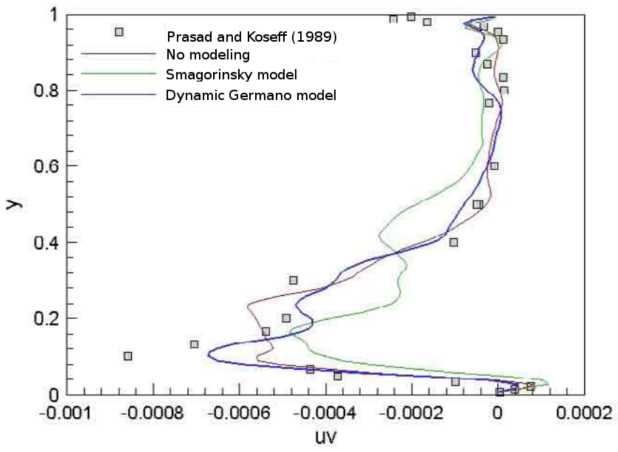

Figure 13: Comparison of UV profiles z = 0.5 and x = to 0.5 and Reynolds number 10000 with literature data.

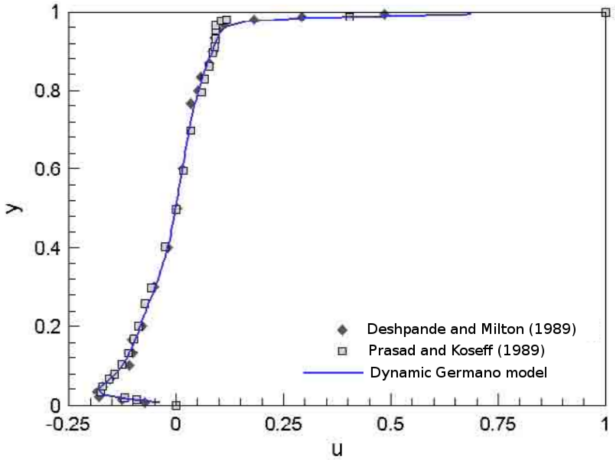

Figure 14: Comparison of profile component of velocity u, z = 0.5 and x = 0.5 for the same Reynolds number 10000 obtained with dynamic modeling with literature data.

eling for the same Reynolds number 3200, indicating that the mesh is insufficient for direct simulation, even for the lowest Reynolds number. Therefore, even in this case, the turbulence modeling is required,

Figure 15 indicates the streamlines plotted in the planes z = 0.12 and z = 0.62. In the foreground, the streamline is a structure with a spiral flow from the center to the outside. However, in planes that intersect the central r e circulating structure, streamline has two distinct motions; the first is external from the center to the periphery, and the second is internal, with opposite direction.

In the flow with Reynolds number 50.000, the bifurcation in the posterior secondary vortex of the mean flow continues to appear, as indicated in Fig. 16. This case presented a blurring at the bifurcation point with streamlines with flows toward the symmetry plane or towards the side walls, depending on whether it is an inner or outer structure. This case also presents a strong asymmetry in the average results in relation to the plane of symmetry, which is probably due to preferential directions adopted in the solution of the correction of the linear system pressure through MSIP method.

Figure 17 illustrates the central line current recirculation of the mean flow with Reynolds number 100000. Observe the recirculation with reverse flow shown in the flow Reynolds number of 50,000. In this case, this recirculation extends to the vicinity of the side wall submitted to deformations peculiar to the regions of the vortex influence and the side of the central counter-rotating structure. The nearest to the plane of

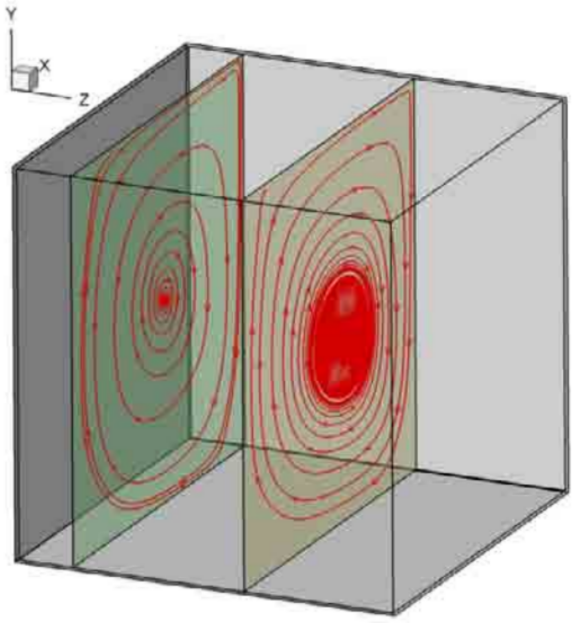

Figure 15: Streamlines in the plans z = 0.12 and z = 0.62 of the flow average for Reynolds number 50000.

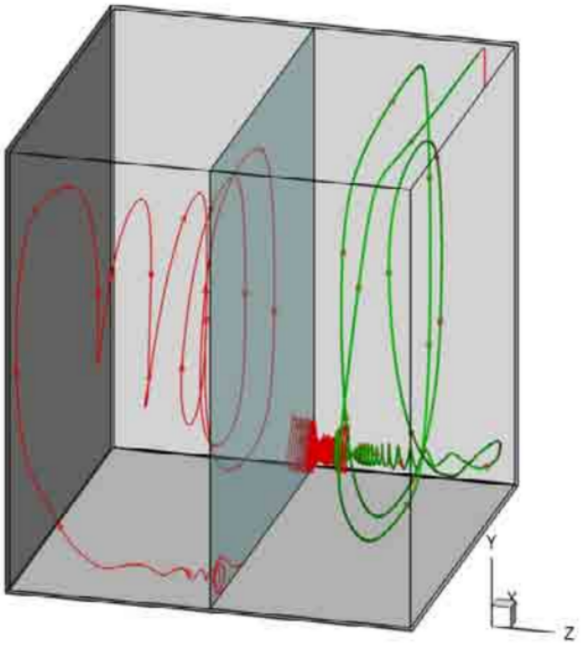

Figure 16: Streamlines in the secondary vortices of the mean flow to Reynolds number thinning 50000.

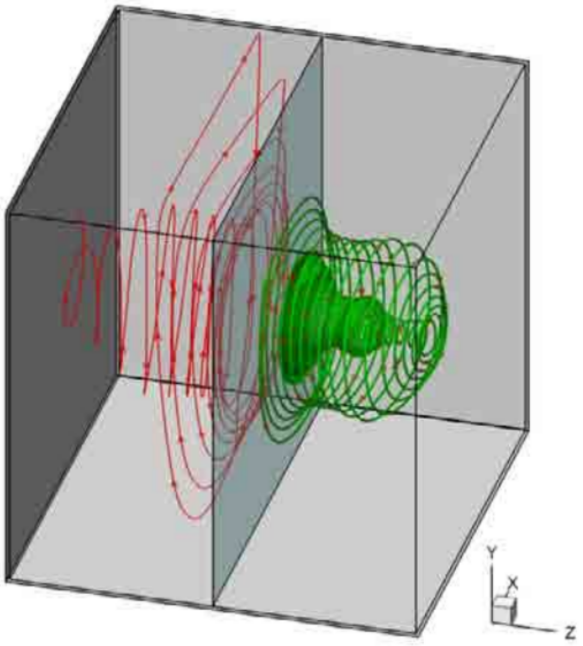

Figure 17: Streamlines in the central recirculation of the mean flow for Reynolds number equal to 100000.

symmetry region suffers thinning both the internal and the external flow. In the vicinity of the internal sidewall, tapers flow and return flow indicated by following the pressure are lateral to the plane of symmetry

In the flow Reynolds number 100000, a flow division process initiated with the bifurcation of the posterior secondary vortex is consolidated, which occurs with the onset of counter-rotating structure. This structure defines a distinct flow pattern by deforming the streamlines to the central circulation,which is indicated in Fig. 17 presenting a very deformed structure.

Figure 18 shows the velocity profile in the direction x. It is observed that the flow at higher Reynolds numbers there is a reverse tendency to increase the value of peak velocity in the lower region. Some factors lead to the conclusion that the behavior described influenced by the presence of counter-rotating structure. First, this mass pumps structure plan for the region symmetry. Second, because this behavior is enhanced in the flow Reynolds number equal to 100,000, wherein the formation is consolidated structure. And finally, because where there is the presence of this structure, as in the posterior region, this behavior is not observed. For comparison, the velocity peaks are indicated in Tab. 1, 2 and 3.

Figures 19 and 20 indicate RMSu (root mean square of velocity u) and RMSv profiles, respectively.

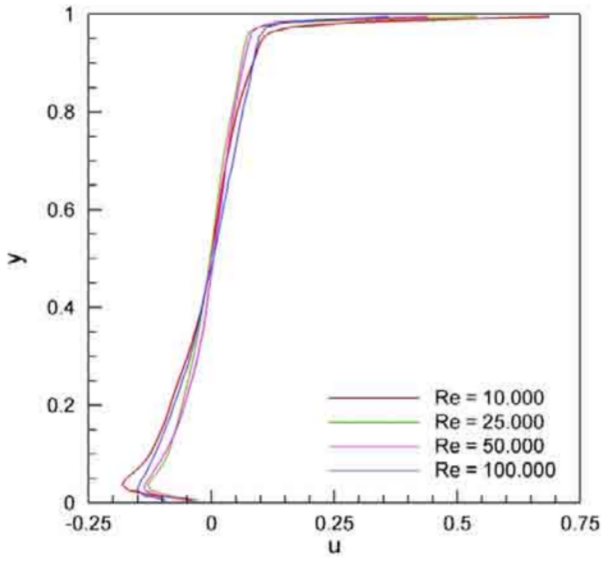

Figure 18: Comparison between the profiles of the velocity component u, z = 0.5 and x = 0.5.

Table 1: Minimum velocity points in the velocity profile in x direction at z = 0.5 and x = 0.5.

Reynolds number	y position	u velocity
10.000	0.0368	0.1815
25.000	0.0368	0.1285
50.000	0.0263	0.1358
100.000	0.0263	0.1517

Observe the highest energy peaks of the lid next to higher Reynolds numbers (Fig. 19). This is an expected behavior; it indicates a smaller influence of the wall on speed fluctuations as the value of this parameter increases. However, in the region close to the posterior wall (Fig. 20)) RMSv, the peaks have opposite behavior, decreasing value and approaching the wall. This behavior is repeated in the lower wall region, a possible explanation is that for higher Reynolds number, most of the fluctuations occur in the smaller ranges shaped for their energy to be not computed.

Table 2: Maximum velocity points in the velocity profile in y direction at z = 0.5 and y = 0.5.

Reynolds number	x position	v velocity
10.000	0.0474	0.1186
25.000	0.0368	0.0904
50.000	0.0368	0.0947
100.000	0.0263	0.1152

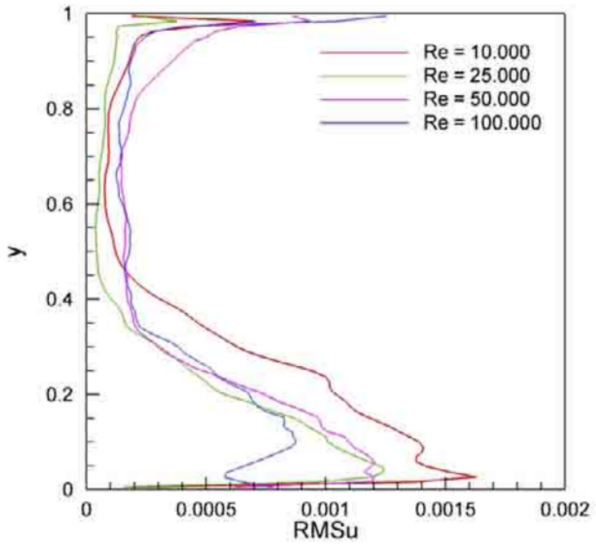

Figure 19: Comparison between the RMSu profiles at z = 0.5 and x = 0.5.

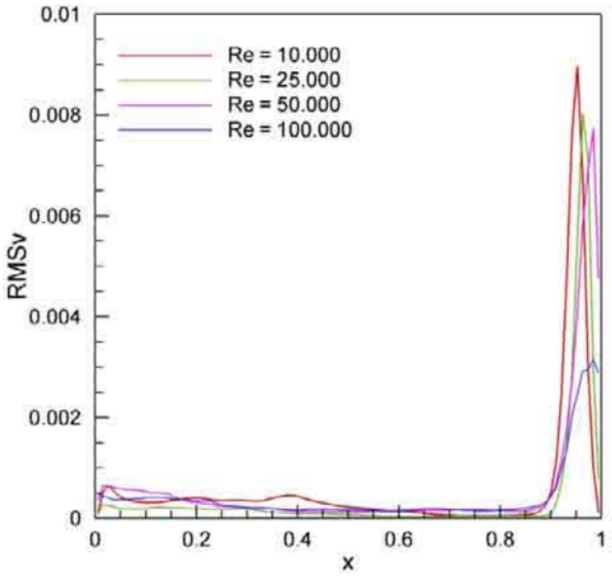

Figure 20: Comparison between the RMSv profiles at z = 0.5 and x = 0.5.

Table 3: minimum velocity points in the velocity profile in y direction at z = 0.5 and y = 0.5.

Reynolds number	x position	v velocity
10.000	0.9737	0.3623
25.000	0.9737	0.3170
50.000	0.9842	0.2462
100.000	0.9737	0.2152

4 Conclusions

The results point that the tool is designed to obtain numerical solutions of Navier-Stokes equations with reliability, both for dimensional and three-dimensional configurations. Results obtained with this tool have good accordance with experimental and numerical results in the literature; however, no results with fourth-order discretization with centered differences are indicated. Regarding the three dimensional case, Reynolds number of cases 3200 and 10000 have values of mean velocity profiles in good accordance with experimental data and data number in the literature. This study simulated flow Reynolds numbers of 25000, 50000 and 100000; these flows presented very different aspects. Flow at Reynolds number 25000 presented topology almost equal to flow Reynolds number 10000, while flow Reynolds number 50000 presented a recirculating structure in the central region of reverse flow to the central recirculation. In addition, this flow presented no well-defined counter-rotating structures of Taylor-Grtler. Flow Reynolds number 100000 presented central recirculation structure with fully developed reverse flow, extending to the vicinity of the side walls. This case is presented under the influence of a pair of counter-rotating structures in the central region, with a toroidal shape, and extend from the bottom wall of the lid cavity to near the front wall. This structure generates a mass flow to the central region, reversing the tendency to decrease the speed peak in the velocity profile in the x direction of the plane of symmetry for Reynolds number up to 25000.

Acknowledgements:

References:

[1] Burggraf, O. R., 1966. "Analitical and numerical studies of the structure of steady separated flow". *Journal of Fluid Mechanics,* **24**(1), Jan, pp. 113–151.

[2] Pan, F., and Acrivos, A., 1967. "Steady flow in rectangular cavities". *Journal of Fluid Mechanics,* **28**(4), Jun, pp. 643–655.

[3] Sheu, T. W. H., and Tsai, S. F., 2002. "Flow topology in a steady three-dimensional lid-driven cavity". *Computers and Fluid,,* **31**, pp. 991–934.

[4] Peng, Y. F., Shiau, Y. H., and Hwang, R. R., 2003. "Transition in a 2-d lid-driven cavity flow". *Computers and Fluids,* **32**, nov, pp. 337–352.

[5] Aidun, C. K., Triantafillopoulus, N. G., and Benson, J. D., 1991. "Global stability of a lid-driven cavity with throughflow: Flow visualization studies". *Phisics and Fluids A,* **3**, pp. 2081–2091.

[6] Shankar, P. N., and Deshpande, M. D., 2002. "Fluid mechanics in the driven cavity". *Annual Reviw of Fluid Mechanics,* **32**, pp. 93–136.

[7] Prassad, A. K., and Koseff, J. R., 1989. "Reynolds number and end-wall effects on a lid-driver cavity flow". *Physics and Fluid A,* **1**, Feb, pp. 208–218.

[8] Chiang, T. P., and and, W. H. S., 1997. "Numerical prediction of eddy structure in a shear-driven cavity". *Computational Mechanics,* **20**, pp. 379–396.

[9] Koseff, J. R., and Street, R. L., 1984. "Visualization of a shear driven of three- dimensional recirculating flow". *Jounal of Fluid Engineering,* **106**, pp. 21–29.

[10] Migeron, C., Pineau, G., and Texier, A., 2003. "Three-dimensionality development inside standard parallelepipedic lid-driven cavities at re = 1000". *Jounal of Fluids and Structure,* **17**, pp. 717–738.

[11] Hassan, Y. A., and Barsamian, H. R., 2001. "New-wall modeling for complex flow using the large eddy simulation technique in curvilinear coordenates". *International Journal of Heat and Mass Transfer,* **44**, pp. 4009–2036.

[12] Germano, M., Piomelli, H., Moin, H., and Cabot, W. H., 1991. "A dynamic subgrid- scale eddy viscosity model". *Phisics and Fluids A,* **3**(7), July, pp. 1760–1765.

[13] Silveira-Neto, A., Grand, D., O, M., and Lesieur, M., 1998. "A numerical investigation of the coherent structures of turbulence behind a backward- facing step". *Journal of Fluid Mechanics,,* **256**, pp. 1–55.

[14] Lesieur, M., Metais, O., and Comte, P., 2005. *Large Eddy-Simulation of Turbulence*. Cambridge University Press.

[15] Maliska, C. R., 1995. *TransferIncia de Calor e Mecnica dos Fluidos Computacional*. Livros Tcnicos e Cientficos Editora.

[16] Schneider, G. E., and Zedan, M., 1981. "A modified strongly implicit procedure for the numerical solution of field problems". *Numerical Heat Transfer,* **14**, pp. 1–19.

[17] Ghia, U., Ghia, K. N., and Schin, C. T., 1982. "High-re solutions for incompressible flow using the navier-stokes equations and a multigrid method". *Jounal of Computational Physics,* **48**, Dez, pp. 387–411.

[18] Hayase, T., Humphrey, J., and Greif, J. A. C. E., 1992. "A consistently formulated quick scheme for fast and stable convergence using finite-volume iterative calculation procedures". *Jounal of Computational Physics,* **98**, pp. 108–118.

[19] Bruneau, C. H., and Saad, M., 2006. "The 2d lid-driven cavity problem revisited". *Computers and Fluids,* **35**, Mar, pp. 326–348.

[20] Jeong, J., and Hussain, F., 1995. "On the identification of a vortex". *Journal of Fluid Mechanics,* **285**, pp. 69–94.

[21] Deshpande, M. D., and Milton, S. G., 1998. "Kolmogorov scale in a driven cavity flow". *Fluid Dynamics Researc,* **22**, pp. 359–381.